High resolution electron energy loss spectroscopy of clean and hydrogen covered Si(001) surfaces: First principles calculations

C. H. Patterson

Citation: The Journal of Chemical Physics **137**, 094701 (2012); doi: 10.1063/1.4748259
View online: http://dx.doi.org/10.1063/1.4748259
View Table of Contents: http://scitation.aip.org/content/aip/journal/jcp/137/9?ver=pdfcov
Published by the AIP Publishing

High resolution electron energy loss spectroscopy of clean and hydrogen covered Si(001) surfaces: First principles calculations

C. H. Patterson[a)]
School of Physics, Trinity College Dublin, Dublin 2, Ireland

(Received 28 April 2012; accepted 14 August 2012; published online 4 September 2012)

Surface phonons, conductivities, and loss functions are calculated for reconstructed (2×1), p(2×2) and c(4×2) clean Si(001) surfaces, and (2×1) H and D covered Si(001) surfaces. Surface conductivities perpendicular to the surface are significantly smaller than conductivities parallel to the surface. The surface loss function is compared to high resolution electron energy loss measurements. There is good agreement between calculated loss functions and experiment for H and D covered surfaces. However, agreement between experimental data from different groups and between theory and experiment is poor for clean Si(001) surfaces. Formalisms for calculating electron energy loss spectra are reviewed and the mechanism of electron energy losses to surface vibrations is discussed.
 [http://dx.doi.org/10.1063/1.4748259]

I. INTRODUCTION

High resolution electron energy loss spectroscopy (HREELS) is an important technique for monitoring surface structure and lattice dynamics through vibrational excitations. Here we report calculations of HREELS spectra of clean and H or D covered Si(001) surfaces. Dimer buckling arrangements of the clean surface with c(4×2), p(2×2), and (2×1) surface unit cells are considered, as well as the (2×1)H and D surfaces. In general, HREELS measures surface phonon dispersion. In a specular scattering geometry (with scattering wavevector $\mathbf{Q}_{||} = 0$), it measures vibrational excitations at semiconductor surfaces via electric-dipole or impact mechanisms.[1] Strong losses in HREELS experiments done in a specular scattering geometry are believed to occur when a surface vibration has a strong dynamic dipole moment perpendicular to the surface.[2] This is sometimes referred to as the surface dipole rule.[3] In early theoretical work,[1,2] Mills and co-workers attributed the absence of scattering by modes with dynamic dipole moments oriented parallel to metal surfaces (or narrow band gap semiconductor surfaces, such as Si) to screening of those moments by the bulk response of the substrate.

Using B3LYP[4,5] hybrid DFT calculations of vibrational modes at clean and H covered Si(001) surfaces, we find that atoms in the first three atomic layers in the Si(001) surface have large Born charges. Born charge tensor components which determine charge displacement *parallel* to the surface in a vibrational mode exceed e in some cases while tensor components for charge displacement *perpendicular* to the surface are much smaller (of order $0.01e$). Displacement of ions parallel to the surface results in large electron transfer between ions in covalent bonds, especially in chemically unsaturated, clean Si(001) surfaces, while displacement of ions perpendicular to the surface does not, in apparent contradiction of the rule mentioned above. The relatively small charge transfer associated with atomic motion perpendicular to the surface, compared to motion parallel to the surface, makes it especially difficult to assign HREELS spectra for complex surfaces. We have previously shown that atomic motions both perpendicular and parallel to the surface contribute to the HREELS dipole scattering cross section of H covered Si(001) surfaces.[6]

There have been surprisingly few reports of HREELS measurements on the clean Si(001) surface in the vibrational[7,8] and interband[9] loss regions. First principles calculations of electron energy losses due to interband transitions at the Si(001) surface were reported recently.[10] Takagi *et al.*[7] and Eremtchenko *et al.*[8] reported room temperature HREELS measurements of the clean Si(001) surface. The dearth of HREELS measurements at this important surface may be due to the low electron scattering cross sections of phonons on the clean Si(001) surface and the tendency for electron beams to disorder the surface at low temperature.[11] HREELS spectra for the Si(001)-(2×1)H and D surfaces were reported recently by Eremtchenko *et al.* in the same paper.[8] These measurements followed earlier work on the Si(001)-(2×1)H surface.[3,12–14] Assignment of H stretching and bending modes for the (2×1)H and D surfaces is straightforward and therefore provides a good test of a first principles calculation of HREELS spectra. Allan and Mele calculated the phonon dispersion relation for the Si(001)-(2×1)H surface[15] with one H atom per surface Si atom. Phonon dispersion relations have been reported for the clean Si(001) surface by Mele and co-workers[16,17] using a tight-binding method, by Fritsch and co-workers[18,19] using a density functional perturbation theory method and by Tütüncü *et al.*[20] using a bond-charge model. Alerhand and Mele also calculated the dipole activities of phonons at the Si(001)-(2×1) surface.[17] Recent STM[21–26] and atomic force microscopy (AFM)[27] studies have shown that the Si(001) surface at low temperature consists of both c(4×2) and p(2×2) domains, with c(4×2) predominating. The surface unit cell of each structure is determined by ordering of buckled dimers in rows. Along a particular row, the direction of dimer tilt alternates along the row. c(4×2) domains result

a)Electronic mail: Charles.Patterson@tcd.ie.

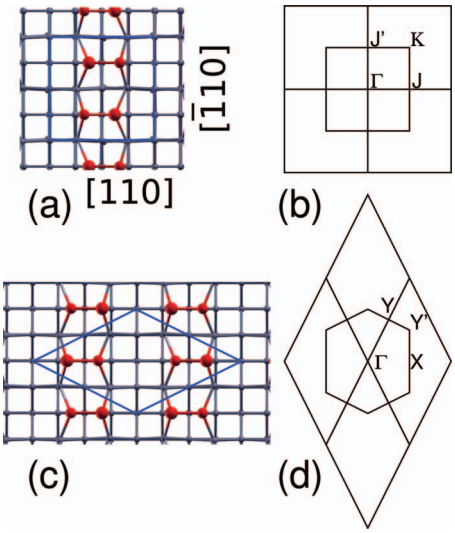

FIG. 1. Real space and reciprocal space unit cells for the Si(001) c(4×2) and p(2×2) surfaces. Real (a) and reciprocal (b) space cells of the p(2×2) dimer arrangement. Real (c) and reciprocal (d) space cells of the c(4×2) dimer arrangement. Dimer rows are shown in red.

when tilting in neighboring rows is out of phase between rows and p(2×2) domains result when tilting is in phase between rows, as shown in Fig. 1.

The remainder of this paper is organized as follows: formalisms used to calculate surface conductivity and HREEL spectra are outlined in Sec. II. This is followed by a section describing the hybrid DFT methods used in this work and a section presenting and discussing results of calculations.

II. THEORY

The theory of electron energy loss at surfaces was initially developed by Lucas and Šunjić[28] and by Evans and Mills.[2,29] The formalism by Mills is given in detail in the book by Ibach and Mills.[1] Lambin, Vigneron, and Lucas[30] adopted an approach in which the energy loss was calculated from the work done by a charged particle as it passes through a dielectric. Approaches based on the first Born scattering approximation adopted by Mills and co-workers,[2,29] Persson,[31] and others and classical approaches by Lucas and co-workers[30,32] come to essentially the same conclusions regarding the scattering cross section. It can be expressed as a product of a kinematic term, A($\mathbf{Q}_{||}$, ω), and a surface loss function term, P($\mathbf{Q}_{||}$, ω),

$$\frac{d^2S}{d\Omega(\hat{k}_S)d\hbar\omega} = A(\mathbf{Q}_{||},\omega)P(\mathbf{Q}_{||},\omega), \tag{1}$$

where

$$A(\mathbf{Q}_{||},\omega) = \frac{2m^2e^2v_\perp^4}{\pi\hbar^5 cos\theta_I}\frac{k_S}{k_I}\frac{|R_I|^2}{[v_\perp^2Q_{||}^2+(\omega-\mathbf{v}_{||}.\mathbf{Q}_{||})^2]^2}, \tag{2}$$

and

$$P(\mathbf{Q}_{||},\omega) = \frac{2\hbar Q_{||}}{\pi}[1+n(\omega)]Im\frac{-1}{\tilde{\epsilon}(Q_{||},\omega)+1}. \tag{3}$$

k_I and k_S are the incident and scattered wavevector magnitudes, θ_I is the incidence angle, R_I is the reflection amplitude for the surface in the absence of any surface vibration and m, e, $\hbar\omega$, and $\mathbf{v}$ are the scattering electron mass, charge, energy, and velocity, respectively. Multiple scattering effects are omitted in the approach used here.

$1+n(\omega)$ is a Bose-Einstein factor, $\mathbf{Q}_{||}$ is the component of the scattering vector parallel to the surface, and $\tilde{\epsilon}(\mathbf{Q}_{||},\omega)$ is an effective dielectric function which contains both surface and bulk responses to the incoming electron. The surface response function, $\tilde{\epsilon}$, in Eq. (3) is derived from a 3-layer model containing a vacuum layer, a thin surface layer of thickness d with dielectric function ϵ_s, and bulk dielectric function ϵ_b. It is given by,[1]

$$\tilde{\epsilon}(Q_{||},\omega) = \epsilon_s(\omega)\frac{1+\Delta(\omega)e^{-2Q_{||}d}}{1-\Delta(\omega)e^{-2Q_{||}d}}, \tag{4}$$

where

$$\Delta(\omega) = \frac{\epsilon_b(\omega)-\epsilon_s(\omega)}{\epsilon_b(\omega)+\epsilon_s(\omega)}. \tag{5}$$

ϵ_s contains the static, electronic contribution to the dielectric function as well as the surface phonon contribution. The phonon contribution to the bulk dielectric constant is zero by symmetry in cubic Si, but at the surface there is an anisotropic contribution from surface localized phonons.

A. Phonon calculations and Born charge tensors

The change in slab polarization, ∂P_i caused by a displacement, $\partial u_{\alpha j}$, of the αth atom, defines the atomic Born charge tensor,

$$Z^*_{\alpha,ij} = \frac{\partial P_i}{\partial u_{\alpha j}}\frac{\Omega}{e}, \tag{6}$$

where Ω is the slab cell volume and charges are in units of the fundamental charge, e. The change in polarization induced by displacements of ions along a phonon coordinate is required for the phonon contribution to the dielectric function and conductivity of the surface. Born charge tensors in the normal (Z) and atomic, Cartesian (Z^*) coordinate systems are related by,

$$Z_{p,i} = \sum_{\alpha,j}\frac{t_{p,\alpha j}Z^*_{\alpha,ij}}{\sqrt{M_\alpha}}, \tag{7}$$

where p labels the vibrational mode, $t_{p,\alpha i}$ contains components of the pth phonon eigenvector, and M_α is the mass of the αth atom.

The bulk, static dielectric contribution to the surface dielectric function is ϵ_b, and the phonon contribution is given in terms of Born charge tensors in the phonon basis and phonon frequencies,

$$\epsilon_{ii}(\omega) = \epsilon_b + \frac{e^2}{\epsilon_o\Omega}\sum_p\frac{Z_{p,i}Z_{p,i}}{\omega_p^2-\omega^2-i\omega\gamma}. \tag{8}$$

ω_p and γ are the frequency of the pth mode and a phenomenological damping parameter.

The phonon contribution to the (diagonal) surface conductivity tensor in S/□ is

$$\sigma_{ii}(\omega) = \frac{e^2}{\epsilon_o A} \sum_p \frac{\gamma \omega^2 Z_{p,i} Z_{p,i}}{\omega_p^2 - \omega^2 - i\omega\gamma}. \quad (9)$$

A is the area of the surface unit cell.

B. Surface electric fields and the scattering potential

Electric fields inside and outside the surface of an ideal dielectric, with dielectric constant ϵ, may be calculated by the method of images.[33] If a charge, Q, in vacuum, is placed above an ideal dielectric, it induces a circularly symmetric positive screening charge at the vacuum/dielectric interface. The total potential of the external plus induced charges, outside the dielectric, is equivalent to that produced by the external charge plus an image charge, $-Q(\epsilon - 1)/(\epsilon + 1)$, inside the dielectric. The total potential inside the dielectric is equivalent to that produced by a single charge, $2Q\epsilon/(\epsilon + 1)$, at the site of the vacuum charge. Electric fields inside and outside the dielectric are therefore,

$$E_\perp^{in} = \frac{2}{\epsilon + 1} E_\perp, \quad (10)$$

$$E_\perp^{out} = \frac{2\epsilon}{\epsilon + 1} E_\perp, \quad (11)$$

$$E_{||}^{in} = E_{||}^{out} = \frac{2}{\epsilon + 1} E_{||}, \quad (12)$$

where $E_\perp$ and $E_{||}$ are components of the field of the charge, Q, in vacuum. The usual boundary conditions for the parallel component of an electric field and perpendicular component of the displacement field at a vacuum/dielectric interface are satisfied. Thus the perpendicular component of the electric field of an electron which is incident on the surface of an ideal dielectric is enhanced by a factor of $2\epsilon/(\epsilon + 1)$ just outside the dielectric, while the parallel component is reduced by a factor $2/(\epsilon + 1)$.

The role of local fields at surfaces in the 3-layer model of the surface loss function can be understood further by expanding it in powers of $Q_{||}d$,[1] as

$$Im \frac{-1}{\tilde{\epsilon}(Q_{||}, \omega) + 1} = Im \frac{-1}{\epsilon_b + 1} + \left[\frac{\epsilon_b^2}{(\epsilon_b + 1)^2} Im \frac{-1}{\epsilon_s} + \frac{1}{(\epsilon_b + 1)^2} Im\epsilon_s \right] Q_{||}d + O(Q_{||}^2 d^2). \quad (13)$$

Electromagnetic modes in bulk solids, such as bulk plasmons, occur at the poles of the inverse bulk dielectric function, $1/\epsilon$. Surface excitations at a vacuum/dielectric interface occur at poles of $1/(\tilde{\epsilon} + 1)$.[34] Electromagnetic mode frequencies of bulk materials with a macroscopic slab geometry are determined by the macroscopic field and the bulk susceptibility, $\chi(\omega) = \Omega_p^2/(\omega_p^2 - \omega^2)$, where ω_p are excitation frequencies and Ω_p is the corresponding plasma frequency. The macroscopic field contains the external field, $E_\perp$, and a depolarizing field, $-P_\perp/\epsilon_o$, created by surface polarization charges. The polarization perpendicular to a slab face is therefore,

$$P_\perp = \epsilon_o \chi \left(E_\perp - \frac{P_\perp}{\epsilon_o} \right), \quad (14)$$

$$P_\perp = \epsilon_o \chi (1 + \chi)^{-1} E_\perp, \quad (15)$$

and it is clear that excitations occur at zeros of $(1 + \chi)$ (or poles of ϵ^{-1}). In the present context, $1 + \chi$ is the sum of the phonon and static, bulk, electronic contributions to ϵ_{ii}. Zeros of $1 + \chi$ occur at

$$\omega^2 = \omega_p^2 + \frac{\Omega_p^2}{\epsilon_b}. \quad (16)$$

Electromagnetic modes polarized parallel to the surface occur at phonon frequencies, $\omega = \omega_p$, i.e., without any shift due to surface local fields. Phonon calculations which are presented below are performed within a self-consistent field approximation which includes the depolarizing field created by surface polarization charges. Hence the shifts in frequencies of modes polarized perpendicular to the surface, Ω_p^2/ϵ_b, are implicitly included in the phonon calculations and ϵ_s^{-1} in Eq. (13) is replaced by ϵ_{zz} in Eq. (17). Terms in Eq. (13) can therefore be interpreted as follows: the term independent of $Q_{||}d$ is the surface response of the semi-infinite bulk layer, which is present even in the absence of a surface layer; the term containing $Im\ \epsilon_s^{-1}$ is the response of the entire surface layer perpendicular to the surface; the term containing $Im\ \epsilon_s$ is the response of the surface layer parallel to the surface. Prefactors containing the bulk dielectric function, ϵ_b, are discussed in Sec. IV C. The surface phonon contribution to the surface loss function, in terms of the dielectric function calculated from Born charges and phonon frequencies is,

$$Im \frac{-1}{\tilde{\epsilon}(Q_{||}, \omega) + 1} = \left[\frac{1}{2(\epsilon_b + 1)^2} Im\epsilon_{xx} + \frac{1}{2(\epsilon_b + 1)^2} Im\epsilon_{yy} + \frac{\epsilon_b^2}{(\epsilon_b + 1)^2} Im\epsilon_{zz} \right] Q_{||}d + O(Q_{||}^2 d^2). \quad (17)$$

A factor $1/2$ has been introduced in the xx and yy terms in Eq. (17) to account for equal proportions of either domain orientation of Si dimers.

III. COMPUTATIONAL METHODS

All electronic structure calculations reported here were performed using the Crystal code.[35] Hybrid DFT calculations used a Hamiltonian similar to that in the B3LYP functional.[4,5] The B3LYP functional contains Hartree-Fock exchange with weight 0.2 and local density and generalized gradient approximations to exchange with combined weight 0.8; this standard functional results in overestimation of the optical band gap of bulk Si. In this work, the relative weight for Hartree-Fock exchange was reduced to 0.05, which results in good agreement with experiment for the value of the static real part and the

position of the $E2$ peak in the imaginary part of the dielectric function of bulk Si.

The Crystal code used in this work employs a finite displacement phonon method[36,37] to calculate the dynamical matrix for $\overline{\Gamma}$ point phonons. Born effective charge tensors in Crystal are obtained using a Berry phase method.[38] Slabs containing 16 Si layers with (2×1), p(2×2), or c(4×2) surface unit cells and both surfaces terminated by Si dimers were used for HREELS calculations of clean Si(001) surfaces. Slabs containing 25 Si layers with (2×1)H or D terminations were used for HREELS calculations of hydrogen covered surfaces. Lattice parameters and atomic coordinates were relaxed until all forces on atoms were below 10^{-4} hartree/bohr. A 6×6 Monkhorst-Pack net[39] was used for all self-consistent field and finite displacement phonon calculations. The Gaussian orbital basis used for Si[40] is described in Ref. 41.

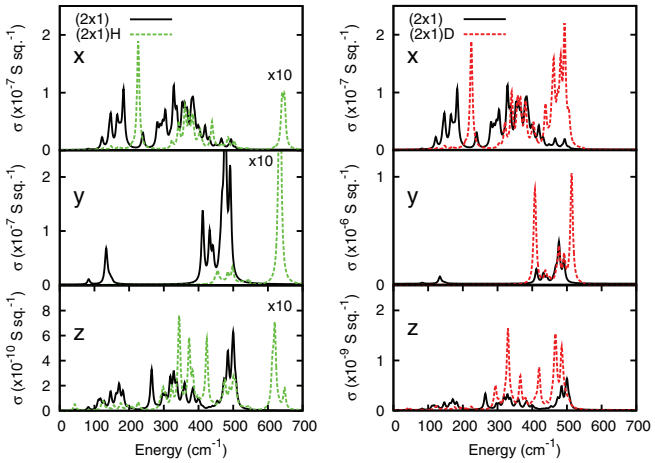

FIG. 2. Conductivities of Si(001)-(2×1), Si(001)-(2×1)H, and Si(001)-(2×1)D. Si(001)-(2×1)H data have been scaled by 1/10 for energies above 550 cm^{-1}. Note differences in scales of coordinate axes.

IV. RESULTS AND DISCUSSION

In this section we present calculations of the phonon contribution to the surface conductivity, the HREELS scattering cross section and analysis of the modes which are responsible for the strongest scattering in HREELS. A limited amount of experimental HREELS data is available for clean Si(001) surfaces. Different primary beam energies are used by Takagi *et al.*[7] and by Eremtchenko *et al.*[8] and near-specular scattering spectra reported by them differ considerably. In order to demonstrate a test of the method used to calculate HREELS spectra, we report spectra for hydrogen covered surfaces and compare them to experimental spectra. HREELS spectra for the Si(001)-(2×1)H and D surfaces have been measured by Eremtchenko *et al.*[8] and by Eggeling *et al.*[3] There is less experimental uncertainty in the composition of the hydrogenated surfaces than the clean surfaces. When a clean Si(001) sample is prepared for an HREELS measurement, (2×1), p(2×2), or c(4×2) domains may coexist and the chemical unsaturation of these surfaces means that they contaminate relatively quickly. On the other hand, provided that the exposure to hydrogen is not too large, surfaces with a single (2×1)H or D reconstruction can be prepared. Furthermore, experimental HREELS data for Si(001)-(2×1)H from several groups are in good agreement.[3,8,12,13] Our calculations of loss energies and intensities are in very good agreement with loss energies and relative intensities from experiment for the hydrogen covered surfaces. This approach can therefore be expected to predict HREELS spectra for clean Si(001) surfaces reliably. The conductivity (Eq. (9)) gives greater weight to high frequency modes than the loss function (Eq. (3)). The latter contains a thermal factor which gives greater weight to modes with $\hbar\omega \leq$ kT and the former contains an extra factor of ω in the numerator of Eq. (9). Consequently, modes with relatively low intensity peaks in the conductivity appear as significant losses in the HREEL spectrum.

A. Si(001)-(2×1)H and D phonons and HREEL spectra

The Si-H(D) symmetric stretching mode is reported at 2090(1525) cm^{-1} by Eremtchenko *et al.*[8] and 2095 cm^{-1} by Eggeling *et al.*[3] We find four modes in the range 2147–2183(1550–1576) cm^{-1} in our calculations for the H(D) covered surfaces. The modes with the largest dipole activities are at 2179(1573) cm^{-1}. Si-H(D) stretching frequencies are therefore overestimated by around 3% when compared to experiment. Bonds to H atoms are strongly anharmonic and the harmonic approximation used here is known to overestimate H atom stretching frequencies. In the case of brucite, $(Mg(OH)_2)$, Pascale and co-workers[42] found the OH stretching frequency was overestimated by around 5% using a B3LYP Hamiltonian and that the stretching frequency agreed with the experimental value within 10 cm^{-1} when allowance was made for anharmonicity of the OH stretching potential.

Surface conductivities up to 700 cm^{-1} for Si(001)-(2×1)H are compared to those for the clean Si(001)-(2×1) surface in Fig. 2. A line broadening parameter, γ, of 5 cm^{-1} was used in conductivity calculations (Eq. (9)). Si dimer bonds are parallel to the [110] (x) direction and dimer rows are parallel to the $[\bar{1}10]$ (y) direction. Frequencies of modes with prominent peaks in the conductivity are given in Table I.

The conductivity parallel to the Si dimer (x) direction at the H covered surface shows a strong peak at 226 cm^{-1} which is the dimer rocking (r) mode and an in-phase Si-H bending mode at 648 cm^{-1}. Allan and Mele report the r mode at

TABLE I. Mode frequencies in cm^{-1} and polarization in the surface conductivity for the Si(001)-(2×1)H and D surfaces.

Polarization	H, ω (cm^{-1})	D, ω (cm^{-1})	Character
x	226	224	Dimer rock
x	648	493	In-phase H/D bend
y	635	407	In-phase H/D bend
y		513	In-phase H/D bend
z	344	330	Anti-phase H/D bend
z	373	420	Anti-phase H/D bend
z	424	468	Anti-phase H/D bend
z	620	484	Anti-phase H/D bend
z	2179	1573	Si-H/D stretch

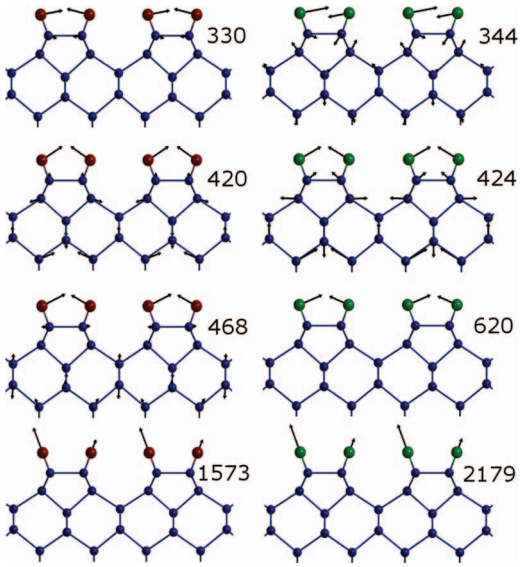

FIG. 3. Phonon eigenvectors for modes at Si(001)-(2×1)D (left) and Si(001)-(2×1)H (right) surfaces with the greatest conductivities perpendicular to the surface plane.

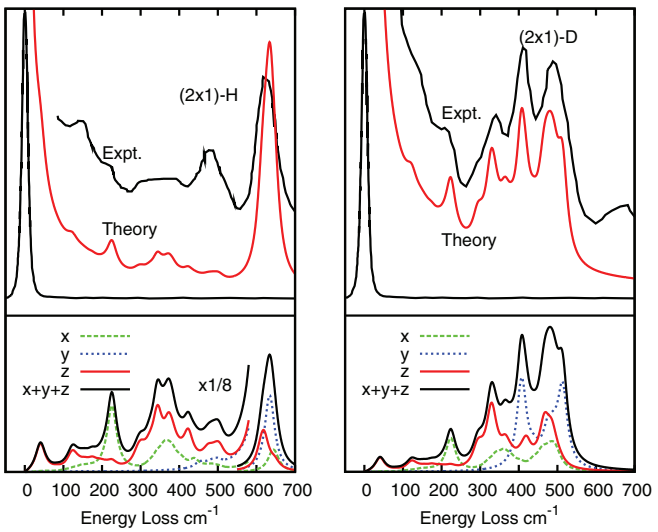

FIG. 4. HREELS loss functions for the Si(001)-(2×1)H and D surfaces (red) and experimental HREELS data (black) from Eremtchenko *et al.*[8] The primary beam energy in the experimental work was 2.5 eV and the incidence angle was 64°. Vertical lines indicate experimental peak positions. Reprinted with permission from C. H. Patterson, Europhys. Lett. **98**, 66001 (2012). Copyright 2012 EPL Association.

210 cm^{-1} at the $\overline{K}$ point of the Brillouin zone.[15] The conductivity parallel to dimer rows (y) shows a strong peak at 635 cm^{-1} which is Si-H bending perpendicular to the Si dimer axis. The conductivity perpendicular to the surface plane (z) shows peaks at 344, 373, 424, 620, and 648 cm^{-1}. Peaks in the range 300–470 cm^{-1} correspond to coupled Si dimer stretching/anti-phase Si-H bending along the Si dimer axis.

Modes with a large conductivity parallel to Si dimer bonds (x) at the D covered surface are found at 224 cm^{-1} and in the range 450–500 cm^{-1}, with the most intense mode at 493 cm^{-1}(Fig. 2). The mode at 224 cm^{-1} is the r mode. The 493 cm^{-1} mode corresponds to the in-phase bending mode observed at 648 cm^{-1} in the H covered surface. Two bending modes with a large conductivity perpendicular to the dimer axis (y) are found at 407 and 513 cm^{-1} and correspond to the single mode at 635 cm^{-1} in the H covered surface. Several Si-D bending/dimer stretching modes with conductivity perpendicular to the surface plane (z) are found at 330, 420, 468, and 484 cm^{-1}. The mode at 620 cm^{-1} in the H covered surface lies above the highest frequency in the bulk Si DOS (which is around 500 cm^{-1}) and is therefore strongly localized on Si-H bonds. The corresponding modes in the D covered surface mix strongly with Si bulk modes since they fall below 500 cm^{-1}.

Phonon eigenvectors of modes with a relatively large conductivity perpendicular to the H and D covered surfaces are shown in Fig. 3. The slab used for these calculations does not have a mirror plane of symmetry perpendicular to the Si dimer axis and so there is no requirement for modes to be odd or even about the dimer axis.

HREEL spectra are calculated using Eq. (17). Absolute values of experimental scattering cross sections are not available and calculated cross sections have been scaled arbitrarily. Weights of contributions from xx, yy, and zz elements of the dielectric functions in Eq. (17) are $1/2(\epsilon_b + 1)^2$, $1/2(\epsilon_b + 1)^2$, and $\epsilon_b^2/(\epsilon_b + 1)^2$, respectively, where ϵ_b has been chosen to be 12. Factors of 1/2 in the xx and yy weights are included as the surface is assumed to consist of equal proportions of the two possible orientations of Si dimer domains. Experimental and computed HREEL spectra for the H and D covered surfaces are compared in Fig. 4. Contributions to the computed HREEL spectra from polarization parallel and perpendicular to the surface are also shown in Fig. 4. A Lorentzian function corresponding to the elastic peak has been added to the calculated HREEL spectra to aid comparison to experiment. This function was not added to the decomposition into x, y, and z contributions in these figures. A line broadening parameter, γ, of 30 cm^{-1} was used in dielectric functions (Eq. (8)) to match the experimental resolution.

Experimental HREELS data from Eremtchenko *et al.*[8] for the H covered surface show losses at 145 and 220 cm^{-1}, a broad hump between 310 and 390 cm^{-1} and a strong, asymmetric loss at 617–622 cm^{-1} . Eggeling *et al.*[3] report a loss at 625 cm^{-1} for the H covered surface. There are relatively weak losses at 140 and 215 cm^{-1} and three distinct, intense losses in the experimental data for the D covered surface at 340, 410, and 490 cm^{-1}. The computed HREEL spectra for the H(D) covered surfaces show weak losses at 124(126) cm^{-1} which are Si-H(D) bending motion coupled to bulk Si motion and may correspond to the experimental losses at 145(140) cm^{-1}.

The dimer rocking modes observed in experiment at 220(215) cm^{-1} are calculated to be at 226(224) cm^{-1}. The lower panels of Fig. 4 show that the rocking mode is associated with polarization parallel to the Si dimer axis only. It therefore breaks the surface dipole rule for HREELS, whereby only modes with polarization perpendicular to the surface plane are observed. The computed spectrum for the H covered surface contains weak contributions from Si-H bending/dimer stretching modes with contributions from both x and z polarizations and must correspond to the broad hump seen in experiment between 310 and 390 cm^{-1}. In contrast,

the D covered surface has three strong loss features in the range 300–500 cm^{-1}. Here there is mixing of Si-D bending and surface Si atom motion. There are weak contributions to the D covered surface HREEL spectrum from modes with *x* polarization and stronger contributions from modes with *y* and *z* polarization. The modes with *y* polarization are Si-D bending perpendicular to the Si dimer axis and the modes with *z* polarization at 330, 420, and 468 cm^{-1} are shown in Fig. 3. There is very good agreement between the calculated and experimental spectra. Since this depends on inclusion of large contributions from polarization parallel to the surface, this provides a further demonstration that the surface dipole rule is invalid for these surfaces.

Surface conductivities (Fig. 2) and HREEL spectra (Fig. 4) of both H covered and clean Si(001) surfaces show strong features in the range 450–500 cm^{-1}. There are no strongly scattering surface modes in this energy range for the H covered surface, but many modes localized in the slab interior make contributions to the scattering at this energy. The relative intensities of the losses around 500 cm^{-1} in our calculations, which we assign to surface resonances of bulk phonons, increased when a thicker slab was used for the phonon calculation. This energy corresponds to the maximum of a strong peak in the bulk phonon density of states[20] and it is present for both the clean and H covered (2×1) surface conductivities along *z* (Fig. 2). Hence an assignment to resonances of bulk states at both clean and H or D covered surfaces seems reasonable. Some of the loss intensity around 500 cm^{-1} in the Si(001)-(2×1)D surface is due to Si-D bending modes, as mentioned above.

B. Si(001) clean surface phonons and HREEL spectra

Allan and Mele[16] report three surface phonons, labelled *r*, *s*, and *sb*, in gaps of the projected bulk phonon density of states of the Si(001)-(2×1) surface. *r* is a dimer rocking mode in which the dimer tilt changes, *s* is a dimer swing motion in which dimers oscillate about axes perpendicular to the surface, and *sb* is a motion of the subsurface bonds. Alerhand amd Mele also refer to a five-fold ring mode[17] in which atoms in five membered rings which include pairs of dimer atoms and atoms immediately below the dimer (subdimer atoms) are in motion. These surface atom motions can couple to bulk Si atom motion in more than one way and we find that a particular kind of surface atom motion makes contributions to the surface conductivity and HREELS spectra in more than one mode. Therefore, more than one peak in a spectrum can be assigned to a dimer swing motion, *s*, etc. Reported frequencies for these modes, converted to cm^{-1}, are given in Table II.

The surface conductivity of the clean Si(001)-(2×1) surface is compared to that for the (2×1)H surface in Fig. 2. The clean surface conductivity parallel to dimers (*x*) is dominated by a group of peaks up to 184 cm^{-1} which are dimer rocking modes. The conductivity along dimer rows (*y*) is large in the clean surface in the range 400–500 cm^{-1} and a peak appears at 134 cm^{-1} when H is removed from the surface. The peaks at 134, 412, and 477 cm^{-1} are *s* modes and a peak at 432 cm^{-1} is an *sb* mode. The *s* modes around 412 cm^{-1} are primarily localized on the upper dimer atom and the atom in the valley between dimers while the *s* mode at 477 cm^{-1} is primarily localized on the lower dimer atom and the valley atom. The conductivity perpendicular to the surface (*z*) has an *r* mode at 265 cm^{-1} and an *sb* mode at 484 cm^{-1}. The clean (2×1) surface has a surface localized mode at 501 cm^{-1} which lies above the bulk phonon DOS and is localized on the lower dimer atom and the backbond atom. This surface state was also reported by several other groups (Table II). However, we do not find a surface localized mode above the bulk DOS in the p(2×2) or c(4×2) surfaces.

TABLE II. Mode frequencies in cm^{-1} for the Si(001)-(2×1) surface.

Reference	Rocking mode, *r*	Swing mode, *s*	Subsurface bond, *sb*
AM[a]	207	356	494
FP[b]	158	337	494
TJS[c]	168	348	527
FP[d]	175		525
TJS[e]	171		513
This work[f]	184	412, 477	501

[a]Allan and Mele $\overline{K}$ point, Ref. 16.
[b]Fritsch and Pavone $\overline{K}$ point, Ref. 18.
[c]Tütüncü, Jenkins, and Srivastava, $\overline{K}$ point, Ref. 20.
[d]Fritsch and Pavone $\overline{\Gamma}$ point, Ref. 18.
[e]Tütüncü, Jenkins, and Srivastava, $\overline{\Gamma}$ point, Ref. 20.
[f]$\overline{\Gamma}$ point.

Conductivities of Si(001)-p(2×2) and c(4×2) surfaces are shown in Fig. 5. Mode frequencies for the c(4×2) surface from this work and earlier work are compared in Table III. Conductivities of these surfaces are very similar along dimers or dimer rows. The conductivity along dimers (*x*) is associated with dimer rocking at 194 and 295 cm^{-1} and *sb* modes at higher frequencies. The conductivity along dimer rows (*y*) is dominated by a mode at 382 cm^{-1}, which is an *s* mode localized on dimer atoms and valley atoms. The c(4×2) surface has strong contributions to the conductivity perpendicular to the surface (*z*) from modes at 295 and 476 cm^{-1}. These are *r* and *sb* modes, respectively. Phonon eigenvectors for several key modes at the (2×1) and c(4×2) surfaces are shown in Fig. 6. The *s* mode at 382 cm^{-1} is quite different from that at 412 or 477 cm^{-1} in the clean (2×1) surface, since motion on the valley atoms is vertical rather than horizontal.

Alerhand and Mele[17] reported conductivities of the (2×1), p(2×2), and c(4×2) Si(001) surfaces using a tight binding method. They found that conductivities were of the same order of magnitude parallel and perpendicular to the surface normal. We find similar magnitudes for conductivities parallel to surfaces, but a magnitude around 100 times smaller for the perpendicular direction. Polarization parallel

TABLE III. Mode frequencies in cm^{-1} for the Si(001)-c(4×2) surface.

Reference	Rocking mode, *r*	Swing mode, *s*	Subsurface bond, *sb*
FP[a]	186		482
This work[b]	194	382	

[a]Fritsch and Pavone $\overline{J}$ point, Ref. 18.
[b]$\overline{\Gamma}$ point.

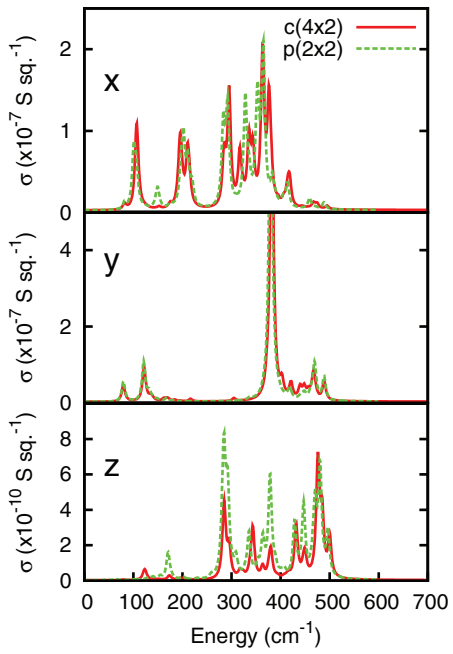

FIG. 5. Conductivities of the Si(001)-p(2×2) and Si(001)-c(4×2) surfaces.

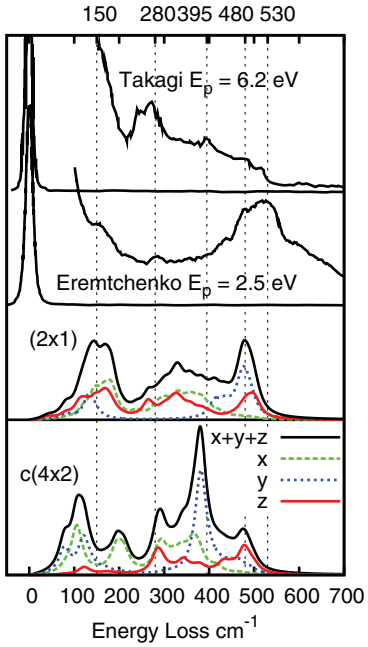

FIG. 7. HREELS spectra for the clean Si(001)-(2×1) and c(4×2) surfaces obtained from the surface loss function and experimental data for clean Si(001) surfaces redrawn from Eremtchenko *et al.*[8] and Takagi *et al.*[7] Primary beam energies and incidence angles in the experimental work by Eremtchenko *et al.* and by Takagi *et al.* were 2.5 eV and 64° and 6.2 eV and 60°, respectively. Vertical lines indicate experimental peak positions referred to in Refs. 7 and 8.

and perpendicular to the surface is obtained self-consistently in our calculations whereas it may not have been in the earlier tight-binding calculations. This may explain the difference in the predictions of the two calculations for polarization perpendicular to the surfaces.

HREELS data for the clean Si(001) surface reported by Takagi *et al.*[7] and by Eremtchenko *et al.*[8] are redrawn in Fig. 7 and compared to the HREELS loss function (Eq. (3)) for the Si(100)-(2×1) and c(4×2) surfaces. Data by Takagi *et al.* were recorded at room temperature using a 2.5 eV primary beam energy.[7] Data by Eremtchenko *et al.* were recorded from a surface which exhibited a (2×1) low energy electron diffraction pattern[8] using a 6.2 eV primary beam energy. Eremtchenko *et al.*[8] report losses at 150, 280, 480, and 530 cm^{-1}. Takagi *et al.*[7] report losses at 97, 161, 242, 266, 395, 476, and 516 cm^{-1}. Both groups assigned modes on the basis of bond charge model calculations for the Si(001)-(2×1) surface by Tütüncü *et al.*[20] although no information on loss intensities was available from the bond charge model calculations. The loss reported by Eremtchenko *et al.* and Takagi *et al.* at 530(516) cm^{-1} could be the *sb* surface mode above the bulk phonon DOS, which we find at 501 cm^{-1} and other groups find between 494 and 527 cm^{-1} (Table II). The loss reported at 480(476) cm^{-1} may be caused by the high density of bulk modes in this region which have some amplitude on surface atoms which carry a nonzero Born charge. Conductivities perpendicular to the H covered and clean (2×1) and c(4×2) surfaces have peaks in this region. The loss reported by Takagi *et al.* at 395 cm^{-1} may be the *s* mode with a strong peak around 382 cm^{-1} in the c(4×2) surface, if there are c(4×2) domains present. The loss at 280 cm^{-1} may be an *r* mode which we find at 265 cm^{-1} in the (2×1) surface and at 295 cm^{-1} in the c(4×2) surface. The loss reported at 150(161) may be an *r* mode which we find at 184 cm^{-1} in the (2×1) surface. Clearly, there are major differences between the two sets of experimental data in Fig. 7 and between the experimental data and results of our calculations. Agreement between theory and experiment is significantly better for the H and D covered Si(001) surfaces.

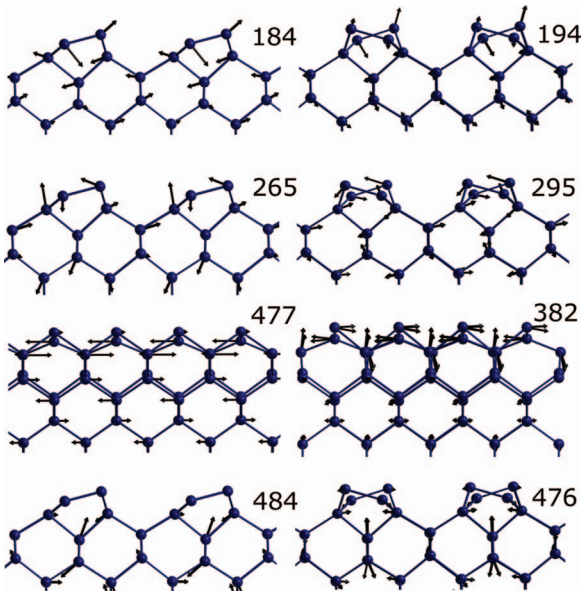

FIG. 6. Phonon eigenvectors for modes at Si(001)-(2×1) (left) and Si(001)-c(4×2) (right) surfaces. Phonon frequencies are given in cm^{-1}.

C. Surface electric fields and charge response

Born charges, which are the average values of diagonal elements of atomic Born charge tensors (Eq. (6)),

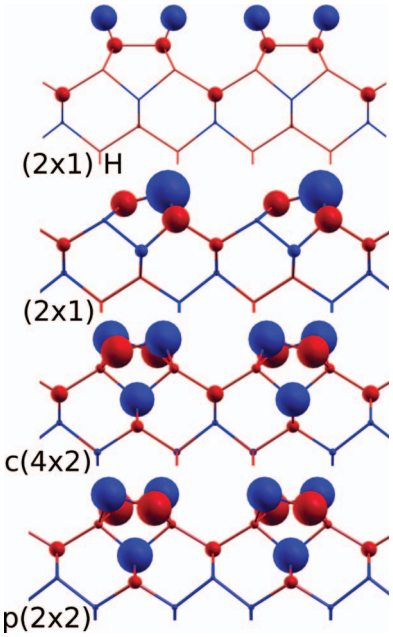

FIG. 8. Born charges at Si(001)-(2×1)H and clean Si(001) surfaces. Sphere radii indicate the magnitude of the Born charge, red is a positive charge and blue negative.

provide a means of understanding the origin of peaks in the surface conductivity and surface loss function since they represent the charge response to atomic displacements. These are shown schematically in Fig. 8 for the four Si(001) surfaces considered in this work. Numerical values for the largest Born charges at these surfaces are given in Table IV and Born charge tensors for atoms in the p(2×2) and (2×1)H surfaces are given in Table V. Born charges are zero by symmetry in bulk Si and can only be nonzero close to the surface. The tensors are highly anisotropic for near-surface atoms and elements governing charge transfer parallel to the surface are around 10 times larger than those governing charge transfer perpendicular to the surface.

Figure 8 and Table IV show that only Si atoms in dimers and first and second layers of any of the surfaces studied have Born charge magnitudes greater than $0.1e$. At the (2×1)H surface, H atoms have the largest charges ($-0.44e$) while the Si dimer has relatively small charges ($0.27e$), compared with buckled, clean surface dimers. In each of the four surfaces studied, the outermost Si atom in the valley between dimer rows has a positive Born charge ranging from $0.24e$ on the clean (2×1) surface to $0.29e$ in the c(4×2) surface. Buckled dimer clean surfaces have large positive charges on the lower

TABLE IV. Born charges for atoms at Si(001) surfaces.

Atom	(2×1)H	(2×1)	c(4×2)	p(2×2)
H	−0.44			
Si dimer up	0.27	−0.75	−0.61	−0.59
Si dimer down	0.27	0.45	0.55	0.59
Si backbond	0.03	0.47	0.17	0.15
Si subdimer	−0.04	−0.22	−0.58	−0.60
Si valley	0.26	0.24	0.29	0.27

TABLE V. Born charge tensors for atoms at the Si(001)-(2×1)H and Si(001)-p(2×2) surfaces. (a) H atom, (b) Si dimer atom, and (c) Si valley atom at the Si(001)-(2×1)H surface. (d) and (e) Outer, inner Si atoms in a tilted Si dimer at the Si(001)-p(2×2) surface and (f) atom immediately below the Si dimer in the Si(001)-p(2×2) surface (see Fig. 8). Born charges for tensors (a)–(f) are −0.41, 0.28, 0.26, −0.59, 0.54, and −0.60, in units of charge, e.

(a) $\begin{pmatrix} -0.45 & 0.00 & 0.00 \\ 0.00 & -0.64 & 0.00 \\ 0.03 & 0.00 & -0.13 \end{pmatrix}$ (b) $\begin{pmatrix} -0.06 & 0.00 & -0.33 \\ 0.00 & 0.75 & 0.00 \\ -0.05 & 0.00 & 0.15 \end{pmatrix}$

(c) $\begin{pmatrix} 0.75 & 0.00 & 0.00 \\ 0.00 & 0.02 & 0.00 \\ 0.00 & 0.00 & 0.01 \end{pmatrix}$ (d) $\begin{pmatrix} -1.29 & 0.00 & -0.55 \\ 0.00 & -0.55 & 0.00 \\ -0.09 & 0.00 & 0.08 \end{pmatrix}$

(e) $\begin{pmatrix} -0.07 & 0.00 & -0.53 \\ 0.00 & 1.69 & 0.00 \\ 0.00 & 0.00 & -0.01 \end{pmatrix}$ (f) $\begin{pmatrix} -1.07 & 0.81 & 0.00 \\ 0.21 & -0.81 & 0.00 \\ 0.00 & 0.00 & 0.07 \end{pmatrix}$

atoms in the dimer and larger negative charges on the upper atoms. There are positive charges on Si backbond atoms and negative charges on atoms immediately below Si dimers. In the (2×1) clean surface there are two types of backbond atom, only the charge for the backbond atoms attached to the dimer up Si atom is given. Subdimer charges in the p(2×2) and c(4×2) surfaces are as large as those in the buckled dimers.

Born charge tensors in Table V for atoms with large Born charges at the surface are highly anisotropic. For all four surfaces studied, the largest elements of the Si dimer tensors are the components corresponding to polarization induced perpendicular to dimers by atom motion in that direction, which is the source of the strong polarization in the s modes described in Sec. IV B.

We have presented calculations of cross sections for dipole scattering by surface modes with small $Q_{||}$ using phonon calculations performed at $Q_{||} = 0$. It is reasonable to assume that the dielectric functions used in calculating HREEL spectra (Eq. (8)) vary slowly with $\mathbf{Q}_{||}$ and that they do not change significantly at values of $\mathbf{Q}_{||}$ used in experiment. For example, Takagi *et al.*[7] used $Q_{||} = 0.06$ Å^{-1} and Eremtchenko *et al.*[8] used $Q_{||} = 0.04$ Å^{-1} for near-specular scattering, which is much closer to $Q_{||} = 0$ than the distance to the nearest surface Brillouin zone boundary (~0.4 Å^{-1} for the p(2×2) surface).

Equations (3) and (4) (and Eq. (17) which is used to calculate HREEL spectra) are derived by considering electric fields propagating into and out of a semi-infinite dielectric with a thin surface layer. The factors $1/(\epsilon_b + 1)^2$ and $\epsilon_b^2/(\epsilon_b + 1)^2$ which appear in the small $Q_{||}d$ expansion of Eq. (3) have been interpreted by Evans and Mills[2] and many subsequent authors, in terms of screening of dipole moments associated with vibrations of atoms in surface layers by the underlying dielectric or metal. The scattering potential in the first Born approximation approach of Evans and Mills,[2] $\Delta_{Q_{||}}(z)$, a distance, z, above a crystal surface at wavevector, $\mathbf{Q}_{||}$ is,

$$\Delta_{Q_{||}}(z) = 4\pi e n_o e^{-Q_{||}z} \frac{\epsilon_b}{1+\epsilon_b} \left(\mathbf{p}_\perp - \frac{i}{\epsilon_b} \hat{\mathbf{Q}}_{||} . \mathbf{p}_{||} \right). \quad (18)$$

n_o is the reciprocal of the surface unit cell area and $\mathbf{p}_\perp$ and $\mathbf{p}_{||}$ are fourier amplitudes which appear in lattice sums of dipole moments oriented normal and parallel to the surface, respec-

tively. $\Delta_{Q_{||}}(z)$ enters the scattering cross section as its modulus squared and so the contribution from $\mathbf{p}_{||}$ is reduced by a factor $1/\epsilon_b^2$ compared to $\mathbf{p}_\perp$ and was neglected by Evans and Mills.[2] The factors containing ϵ_b in the scattering potential are consistent with the screened potential created in vacuum when an electric dipole oriented parallel or perpendicular to the surface is placed just outside an ideal dielectric.[2] Hence the currently accepted picture of the dipole mechanism for charge scattering by surface vibrations is that screening of phonon-induced polarization parallel to the surface results in negligible dipole scattering by vibrations which have atomic motion parallel to the surface and only vibrations which have atomic motion perpendicular to the surface are observed in HREEL spectra. This has come to be known as the surface dipole rule in HREELS[1] and it depends on screening of charges induced by atomic motions associated with surface phonons.

Figure 8 shows that Born charges at clean or H covered Si(001) surfaces are confined to the outermost atomic layers. Components of Born charge tensors (Table V) are large ($\sim e$) for atom displacements parallel to the surface. They are smaller, by up to an order of magnitude, for atom displacements perpendicular to the surface. When an atom is displaced parallel to the surface a large charge transfer may occur, e.g., between dimer atoms, especially at the clean surface where occupied and vacant surface states are localized on the "up" and "down" atoms in the dimer, respectively. Table V shows that when an atom is displaced perpendicular to the surface, the zz component of the Born charge tensor is relatively small, especially for the clean surfaces studied. Presumably this is because an atom, which is displaced perpendicular to the surface, moves (almost) as a neutral atom, rather than because of compensation by charge displacement on neighboring atoms in the opposite sense. The relatively large xx and yy and smaller zz components of dielectric functions and surface conductivities are the opposite of what would be expected, were the currently accepted picture and the surface dipole rule to apply. It should be noted that Born charge tensors express the response of the electronic charge to atomic displacements rather than to an external electric field and so there is actually no requirement for these charges to be screened in the way that the field of an external charge is screened by a dielectric surface. Surface atom Born charge tensors represent an intrinsic response property of the surface to surface atom displacements.

An alternative interpretation of the factors $1/(\epsilon_b + 1)^2$ and $\epsilon_b^2/(\epsilon_b + 1)^2$ in Eq. (17) can be given in terms of parallel and perpendicular components of the electric field strength of the scattering electron in the surface region, where Born charges are large. A dielectric surface treated quantum mechanically can be expected to have near ideal dielectric behavior, provided that the perturbing charge is in the vacuum region and is at least several interatomic spacings away from the surface. In this case the electronic charge responds to the field of a point charge rather than an atomic displacement. As noted in Eqs. (10)–(17), the electric field component parallel to the surface is reduced by a factor $2/(\epsilon_b + 1)$, compared to the field of the bare charge in vacuum, both inside and outside the dielectric surface. On the other hand, the field component perpendicular to the surface is enhanced by a factor $2\epsilon_b/(\epsilon_b + 1)$ outside the layer of screening charge and reduced by a factor $2/(\epsilon_b + 1)$ inside. Since field-field (or equivalently charge density-density) correlation functions appear in the scattering cross section, these factors are squared in the scattering cross section.[1] This interpretation also accounts for the fact that vibrational modes of adsorbates on metals with atomic motions parallel to the surface are not observed in near-specular HREEL spectra,[43] since the parallel component of the electric field is completely screened at a perfect metal surface.

The charge which accumulates at a surface in response to the field of an external charge is expected to reside on the outermost atomic layer(s). Some atoms with large Born charges will therefore lie outside that charge layer and others within it. The actual field at the surface, which is the field driving the response of the surface phonons, requires a microscopic calculation, but this is beyond the scope of the current work. However, good agreement between experimental and calculated HREEL spectra for H and D covered surfaces, where there is relatively little uncertainty in surface structure and surface contamination is not a major experimental problem, suggests that Eq. (17) can be used to calculate HREEL spectra of clean and adsorbate covered semiconductor surfaces. Equation (17) requires only Born charges in phonon coordinates and phonon frequencies, both of which can easily be calculated for semiconductors and insulators using various electronic structure codes. Since both the parallel and perpendicular components of polarization induced by surface phonons can be observed via HREELS, it is not sufficient to assign spectra by searching for modes with atomic motion predominantly perpendicular to the surface. Instead, Eq. (17) can be used to predict and assign spectra.

V. SUMMARY

Symmetry breaking at the surface makes it possible to observe vibrations at the surface of a cubic material such as Si via techniques such as HREELS or infrared absorption which depend on creation of a dynamic dipole moment by the vibration. Motions of atoms in the first three or four layers of the surface induce dipole moments in the surface region while motions of atoms deeper in the solid induce none (by symmetry). We find that components of dynamic dipole moments parallel to the surface are larger than those perpendicular to the surface by an order of magnitude, or so. This finding apparently contradicts the generally accepted idea that only vibrations with dynamic dipole moments perpendicular to the surface are observed in HREELS. This is because any dipole moment parallel to the surface of a dielectric, just outside the surface, is heavily screened. The surface loss function is calculated using a three layer model. This model contains screening factors for dynamic dipole moments parallel and perpendicular to the surface. There is good agreement with HREELS experiment of the H and D covered surfaces, provided that contributions from phonons with dynamic dipole moments parallel to the surface are included.

We have calculated surface conductivities and HREELS spectra for clean Si(001) and H and D covered Si(001)-(2×1) surfaces. HREEL spectra for the H and D covered surfaces

are in good agreement with experiment. However, experimental data[7,8] for the clean Si(001) surface are not in agreement and there are significant differences between calculated (2×1) and c(4×2) HREEL spectra and between calculated and experimental spectra. Differences between experimental spectra may arise because of different primary beam energies (6.2 versus 2.5 eV), differences in surface preparation leading to different dimer arrangements, domain sizes, etc. or even differences in levels of surface contamination. Measurement of HREEL spectra of a single domain Si(001)-c(4×2) surface, prepared using appropriate techniques[44] is needed. Comparison to our calculations, which predict a strong loss feature due to the dimer swing mode at 382 cm^{-1}, would provide a further test of this method for calculating and assigning HREEL spectra and the validity of the surface dipole rule at clean and adsorbate covered semiconductor surfaces.

ACKNOWLEDGMENTS

This work was supported by Science Foundation Ireland under Grant No. RFP/11/PHY/3047. Computer time was provided by the Trinity Centre for High Performance Computing which is supported by the Irish Higher Education Authority and Science Foundation Ireland. The author wishes to acknowledge helpful discussions with John McGilp and Conor Hogan.

[1] H. Ibach and D. L. Mills, *Electron Energy Loss and Surface Vibrations* (Academic, New York, 1982).
[2] E. Evans and D. L. Mills, Phys. Rev. B **5**, 4126 (1972).
[3] J. Eggeling, G. R. Bell, and T. S. Jones, J. Phys. Chem. B **103**, 9683 (1999).
[4] A. D. Becke, J. Chem. Phys. **98**, 5648 (1993).
[5] P. J. Stephens, F. J. Devlin, C. F. Chabalowski, and M. J. Frisch, J. Phys. Chem. **98**, 11623 (1994).
[6] C. H. Patterson, Europhys. Lett. **98**, 66001 (2012).
[7] N. Takagi, S. Shimonaka, T. Aruga, and M. Nishijima, Phys. Rev. B **60**, 10919 (1999).
[8] M. Eremtchenko, F. S. Tautz, R. Öttking, and J. A. Schaefer, Surf. Sci. **600**, 3446 (2006).
[9] H. H. Farrell, F. Stucki, J. Anderson, D. J. Frankel, G. J. Lapeyre, and M. Levinson, Phys. Rev. B **30**, 721 (1984).
[10] L. Caramella, C. Hogan, G. Onida, and R. DelSole, Phys. Rev. B **79**, 155447 (2009).
[11] M. Matsumoto, K. Fukutani, and T. Okano, Phys. Rev. Lett. **90**, 106103 (2003).
[12] J. A. Schaefer, F. Stuckl, J. A. Anderson, G. J. lapeyre, and W. Göpel, Surf. Sci. **140**, 207 (1984).
[13] R. Butz, E. M. Oellig, H. Ibach, and H. Wagner, Surf. Sci. **147**, 343 (1984).
[14] F. S. Tautz and J. A. Schaeffer, J. Appl. Phys. **84**, 6636 (1998).
[15] D. C. Allan and E. J. Mele, Phys. Rev. B **31**, 5565 (1985).
[16] D. C. Allan and E. J. Mele, Phys. Rev. Lett. **53**, 826 (1984).
[17] O. L. Alerhand and E. J. Mele, Phys. Rev. B **35**, 5533 (1986).
[18] J. Fritsch and P. Pavone, Surf. Sci. **344**, 159 (1995).
[19] J. Fritsch and U. Schröder, Phys. Rep. **309**, 209 (1999).
[20] H. M. Tütüncü, S. J. Jenkins, and G. P. Srivastava, Phys. Rev. B **56**, 4656 (1997).
[21] K. Hata, S. Yoshida, and H. Shigekawa, Phys. Rev. Lett. **89**, 286104 (2002).
[22] M. Ono, A. Kamoshida, N. Matsuura, E. Ishikawa, T. Eguchi, and Y. Hasegawa, Phys. Rev. B **67**, 201306 (2003).
[23] K. Sagisaka, D. Fujita, and G. Kido, Phys. Rev. Lett. **91**, 146103 (2003).
[24] K. Sagisaka, D. Fujita, G. Kido, and N. Koguchi, Surf. Sci **566**, 767 (2004).
[25] L. Perdigäo, D. Deresmes, B. Grandidier, M. Dubois, C. Delerue, G. Allan, and D. Stiévenard, Phys. Rev. Lett. **92**, 216101 (2004).
[26] S. Yoshida, T. Kimura, O. Takeuchi, K. Hata, H. Oigawa, T. Nagamura, H. Sakama, and H. Shigekawa, Phys. Rev. B **70**, 235411 (2004).
[27] Y. J. Li, H. Nomura, N. Ozaki, Y. Naitoh, M. Kageshima, Y. Sugawara, C. Hobbs, and L. Kantorovich, Phys. Rev. Lett. **96**, 106104 (2006).
[28] A. A. Lucas and M. Sunjic, Phys. Rev. Lett. **26**, 229 (1971).
[29] D. L. Mills, Surf. Sci. **49**, 59 (1975).
[30] P. Lambin, J. P. Vigneron, and A. A. Lucas, Phys. Rev. B **32**, 8203 (1985).
[31] B. N. J. Persson, Sol. State Commun. **24**, 573 (1977).
[32] P. Senet, P. Lambin, J. P. Vigneron, I. Derycke, and A. A. Lucas, Surf. Sci. **226**, 307 (1990).
[33] P. Lorrain and D. Corson, *Electromagnetic Fields and Waves* (Freeman, San Francisco, 1970).
[34] J. M. Pitarke, V. M. Silkin, E. V. Chulkov, and P. M. Echenique, Rep. Prog. Phys. **70**, 1 (2007).
[35] R. Dovesi, V. R. Saunders, C. Roetti, R. Orlando, C. M. Zicovich-Wilson, F. Pascale, B. Civalleri, K. Doll, N. M. Harrison, I. Bush, P. D'Arco, and M. Llunell (2009), CRYSTAL09 User's Manual, University of Torino, Torino, 2009.
[36] F. Pascale, C. Zicovich-Wilson, F. Lopez, B. Civalleri, R. Orlando, and R. Dovesi, J. Comput. Chem. **25**, 888 (2004).
[37] C. Zicovich-Wilson, F. Pascale, C. Roetti, V. Saunders, R. Orlando, and R. Dovesi, J. Comput. Chem. **25**, 1873 (2004).
[38] S. Dall'Olio, R. Dovesi, and R. Resta, Phys. Rev. B **56**, 10105 (1997).
[39] H. Monkhorst and J. D. Pack, Phys. Rev. B **13**, 5188 (1976).
[40] J. E. Jaffe and A. C. Hess, Phys. Rev. B **48**, 7903 (1993).
[41] F. Pascale, M. Catti, A. Damin, R. Orlando, V. Saunders, and R. Dovesi, J. Phys. Chem. B **109**, 18522 (2005).
[42] F. Pascale, S. Tosoni, C. Zicovich-Wilson, P. Ugliengo, R. Orlando, and R. Dovesi, Chem. Phys. Lett. **396**, 308 (2004).
[43] W. Ho, R. F. Willis, and E. W. Plummer, Phys. Rev. Lett. **72**, 1463 (1978).
[44] R. Shioda and J. vanderWeide, Phys. Rev. B **57**, R6823 (1998).